

University of Groningen

## Free-standing nanolayers based on Ru silicide formation on Si(100)

TrogliA, Alessandro; Van Vliet, Stefan; Yetik, Görsel; Wakil, Ibrahim El; Momand, Jamo; Kooi, Bart J.; Bliem, Roland

*Published in:*  
Physical Review Materials

*DOI:*  
[10.1103/PhysRevMaterials.6.043402](https://doi.org/10.1103/PhysRevMaterials.6.043402)

**IMPORTANT NOTE: You are advised to consult the publisher's version (publisher's PDF) if you wish to cite from it. Please check the document version below.**

*Document Version*  
Publisher's PDF, also known as Version of record

*Publication date:*  
2022

[Link to publication in University of Groningen/UMCG research database](#)

*Citation for published version (APA):*

TrogliA, A., Van Vliet, S., Yetik, G., Wakil, I. E., Momand, J., Kooi, B. J., & Bliem, R. (2022). Free-standing nanolayers based on Ru silicide formation on Si(100). *Physical Review Materials*, 6(4), [043402]. <https://doi.org/10.1103/PhysRevMaterials.6.043402>

### Copyright

Other than for strictly personal use, it is not permitted to download or to forward/distribute the text or part of it without the consent of the author(s) and/or copyright holder(s), unless the work is under an open content license (like Creative Commons).


The publication may also be distributed here under the terms of Article 25fa of the Dutch Copyright Act, indicated by the "Taverne" license. More information can be found on the University of Groningen website: <https://www.rug.nl/library/open-access/self-archiving-pure/taverne-amendment>.

### Take-down policy

If you believe that this document breaches copyright please contact us providing details, and we will remove access to the work immediately and investigate your claim.

*Downloaded from the University of Groningen/UMCG research database (Pure): <http://www.rug.nl/research/portal>. For technical reasons the number of authors shown on this cover page is limited to 10 maximum.*

## Free-standing nanolayers based on Ru silicide formation on Si(100)

Alessandro Troglia<sup>1</sup>, Stefan van Vliet<sup>1</sup>, Görsel Yetik<sup>1</sup>, Ibrahim El Wakil<sup>1</sup>, Jamo Momand<sup>2</sup>, Bart J. Kooi<sup>2</sup>, and Roland Bliem<sup>1,3,\*</sup><sup>1</sup>Advanced Research Center for Nanolithography, Science Park 106, 1098 XG Amsterdam, The Netherlands<sup>2</sup>Zernike Institute for Advanced Materials, University of Groningen, Nijenborgh 4, 9747 AG Groningen, The Netherlands<sup>3</sup>Institute of Physics, University of Amsterdam, Science Park 904, 1098XH Amsterdam, The Netherlands (Received 12 January 2022; revised 22 March 2022; accepted 23 March 2022; published 15 April 2022)

Free-standing layers of nanoscale thickness are essential in numerous applications but challenging to fabricate for all but a small selection of materials. We report a versatile, chemical-free pathway of exfoliating centimeter-sized free-standing nanolayers from Si(100) with native oxide based on the spontaneous delamination of thin Ru and Ru-based films upon annealing at temperatures as low as 400 °C. Combining results from x-ray photoelectron spectroscopy (XPS), and transmission and scanning electron microscopy (TEM, SEM), we identify that the element Ru, a thin SiO<sub>2</sub> layer, and the Si(100) substrate are essential ingredients for the delamination and propose a stress-based mechanism to explain the effect. The diffusion of Si into the layer upon annealing leads to the formation of a Ru-Si compound at the thin-film side of the Ru/Si(100) interface and pyramidal cavities in the Si(100) substrate. Moreover, the uptake of Si results in an increase in layer thickness and the buildup of in-plane compressive stress, which is reduced by local buckling and finally by the separation of the full layer from the substrate at the SiO<sub>2</sub>-Si(100) interface. The use of a thin Ru-buffer layer allows us to apply this delamination process to produce free-standing nanolayers of Mo and HfMoNbTiZr in this simple, chemical-free, and vacuum-compatible manner. These results indicate the potential of the reported effect for the fabrication of free-standing layers using a wide range of compositions, deposition techniques, and growth conditions below the onset temperature of delamination.

DOI: [10.1103/PhysRevMaterials.6.043402](https://doi.org/10.1103/PhysRevMaterials.6.043402)

## I. INTRODUCTION

Thin free-standing membranes are indispensable in technological applications such as frequency filters [1–3], advanced electronics [4,5], gas-separation membranes [6,7], or transparent sheets for short-wavelength radiation [8–11]. They also find application in catalysis [12,13], as electrodes in advanced battery concepts [14–16], and as interconnects [17]. Each of these applications has its own, demanding set of requirements to the respective free-standing films. Customized materials are thus required for good functionality. Manufacturing customized layers in a reproducible way is challenging and often requires complex processing and the intensive use of chemicals, for example for the chemical removal of the entire substrate after depositing the thin films. New, chemical-free ways of producing free-standing films would contribute to developing simpler and more sustainable production methods with a better environmental footprint and potentially a lower price.

The production of free-standing layers typically starts with the deposition of a thin film on the substrate of choice. Thin-film growth is typically accompanied by the buildup of stress,

which finds its origin in intrinsic and extrinsic sources [18,19]. Intrinsic stress is attributed to the formation of defects in the layer during grain growth and to the coalescence of grains. It increases with film thickness and is specific to the combination of deposited material, substrate, and growth conditions [18]. Extrinsic stress components, on the other hand, are not directly related to the atomic-scale structure of a film, but originate for example in the difference in thermal expansion coefficients between the substrate and a film deposited at elevated temperature [19,20]. The superposition of these stress components compromises the adhesion of the film to the substrate and can lead to failure in the form of cracking or uncontrolled delamination if a critical stress value is exceeded.

The stress in a layer of a defined phase and composition varies substantially if its density and structure are modified by processes such as diffusion, intercalation [21], phase transformations [19], and compound formation [22,23]. The formation of silicides by annealing thin films of transition metals deposited onto Si is a good example of this process [24]. The formation of a silicide by Si diffusion typically leads to compressive stress in the layer due to the addition of material, which usually requires a volume expansion to match the different density of the compound formed. Various relaxation mechanisms may lead to a reduction of the total stress in the film [25].

In this article we report the observation that Ru-based metal films on native-oxide-terminated Si(100) substrates delaminate spontaneously at the Si(100)-SiO<sub>2</sub> interface upon

\*r.bliem@arcnl.nl

Published by the American Physical Society under the terms of the [Creative Commons Attribution 4.0 International](https://creativecommons.org/licenses/by/4.0/) license. Further distribution of this work must maintain attribution to the author(s) and the published article's title, journal citation, and DOI.

annealing at approximately 400 °C, yielding centimeter-scale free-standing layers with thicknesses starting at 20 nm. We further observed that a Ru silicide phase was formed by Si diffusion through the native SiO<sub>2</sub> layer during annealing. The uptake of Si substantially increased the equilibrium volume of the film, adding a strong compressive component to the stress in the layer and at the interface. We propose that this buildup of compressive stress is at the root of the delamination and causes the Ru-Si/SiO<sub>2</sub>/Si(100) stack to cleave at the Si-SiO<sub>2</sub> interface. This mechanism reconciles our observations on thin films of various thicknesses and compositions, grown using two different techniques. Moreover, we demonstrate that Mo and HfMoNbTiZr films on Si(100) with an ultrathin Ru silicide buffer layer follow the same delamination pattern, indicating a potential application of the reported Ru-based delamination for the chemical-free exfoliation of customized free-standing metal layers via a versatile, vacuum-compatible, and environmentally friendly process.

## II. METHODS

*Sample preparation:* Pure Ru, Mo, and Ru<sub>100-x</sub>Mo<sub>x</sub> alloy thin films were sputter-deposited onto *p*-doped Si(100) substrates with native oxide using a Polyteknik Flextura M506 S system. The substrates were cleaned with a sequential ultrasonic bath of acetone and isopropanol; the native oxide of Si was not removed prior to deposition. The base pressure of the system was approximately  $1.0 \times 10^{-7}$  mbar. Pure Ru and Mo thin films were deposited by DC sputtering with a power of 200 and 75 W and Ar background pressure of  $2.0 \times 10^{-3}$  and  $1.33 \times 10^{-2}$  mbar, respectively. Ru<sub>100-x</sub>Mo<sub>x</sub> alloy thin films were co-deposited from separate sources by RF and DC sputtering, respectively, with an argon background pressure of  $2 \times 10^{-3}$  mbar. During deposition, the substrates were kept at room temperature and rotated in order to optimize the homogeneity of the deposition. The Ru silicide reference sample was synthesized by depositing a 25 nm thick Ru thin film onto clean Si(100) substrates with native oxide by pulsed laser deposition using a KrF excimer laser at an energy density of 7.5 J/cm<sup>2</sup> and laser repetition rate of 10 Hz. A 99.95% pure Ru target (Alineason Materials Technology GmbH) was used for the deposition process. The substrate was kept at room temperature and the background deposition pressure was  $1.0 \times 10^{-9}$  mbar. The Ru thin film was subsequently annealed at 550 °C to ensure homogeneous conversion of the entire film to Ru silicide [26]. HfMoNbTiZr thin films were deposited with pulsed laser deposition in  $4.0 \times 10^{-2}$  mbar Ar background pressure at an energy density of 11.0 J/cm<sup>2</sup> and a laser repetition rate of 10 Hz. A custom-made HfMoNbTiZr (20:20:20:20 at.%) target was used for the deposition process.

*X-ray photoelectron spectroscopy:* The step-by-step XPS investigation of the delamination process was performed *in situ* in a UHV setup (base pressure better than  $1.0 \times 10^{-9}$  mbar) equipped with a Scienta Omicron R4000 HiPP-3 analyzer (swift acceleration mode, 1 mm slit entrance) and a monochromatic Al-K $\alpha$  source (1486.6 eV). An as-grown Ru thin film (thickness approximately 100 nm) was loaded in the setup via a load lock: the annealing treatment was performed in UHV at approximately 400 °C with a radiative

heater; the temperature was measured both with a thermocouple and a pyrometer. The delamination of the Ru thin film was performed directly in UHV with carbon tape, allowing the XPS measurement of the film-substrate interface side of the delaminated layer and bare substrate separately, avoiding any surface contamination due to air exposure. Survey spectra were recorded at 500 eV of pass energy (PE), while detailed spectra were recorded at PE = 100 eV.

*Scanning electron microscopy:* SEM measurements were performed using a FEI Verios 460 SEM system with a Schottky field electron gun. The SEM micrographs were taken at an electron energy of 5 keV and a beam current of 100 pA. The immersion field mode was used in order to optimize the spatial resolution.

*Transmission electron microscopy:* Cross sectional specimens of the Ru<sub>47</sub>Mo<sub>53</sub> thin film were prepared with an FEI Helios G4 CX dual beam system at 30 kV ion energy and polished at 5 and 2 keV to remove residual surface damage. These specimens were analyzed with a double-aberration-corrected FEI Themis Z scanning transmission electron microscopy system at 300 kV. EDX spectrum mapping was performed with a probe current of 1 nA, where the spectra were recorded with a Dual-X system, providing in total 1.76 sr EDX detector.

## III. RESULTS AND DISCUSSION

Figure 1 depicts a schematic of the observed delamination of Ru thin films upon annealing. After sputter deposition of Ru on native-oxide terminated Si(100), as described in the Methods section, the 20 to 200 nm thick Ru films were found to detach completely from the substrate upon annealing at 400 °C. This delamination was characterized by visible changes in the appearance of the films. The film surface developed visible patches of lower reflectivity and higher apparent roughness. These modified areas expanded, propagating across the sample on a timescale of several seconds and finally leading to a changed appearance of the entire film (see movie in the Supplemental Material [27]). What seemed to be a roughening transition was concomitant with a loss of adhesion between the substrate and the entire Ru layer. The resulting free-standing nanolayers were harvested from the substrate using adhesive tape. For thicknesses of 100 nm and higher, centimeter-sized flakes were directly exfoliated with tweezers, as shown in Fig. 1(c).

The composition and chemical properties of the exposed Si(100) substrate and the thin-film side of the Ru/Si(100) interface were investigated *in situ* after delamination of a 100 nm thick Ru film in ultrahigh vacuum (UHV) by means of x-ray photoelectron spectroscopy (XPS). The survey spectrum of the 100 nm thick Ru film (Fig. S1 [27]) shows only peaks corresponding to Ru and oxygen, which was present due to exposure to air before annealing, whereas Ru, O, and Si were observed at the thin-film side of the interface (Fig. S2 [27]). Figure 2(a) shows the XPS spectra of the extended Ru 3*d* region of the as-grown Ru thin film before annealing (black), the thin-film side of the Ru/Si(100) interface after annealing and delamination in UHV (red), and a separately prepared, thin Ru silicide film that was used as a reference specimen (blue). The spectrum of the as-grown Ru thin film is characterized by the Ru 3*d*<sub>5/2</sub> peak at a binding energy of 279.9 eV, a doublet peak

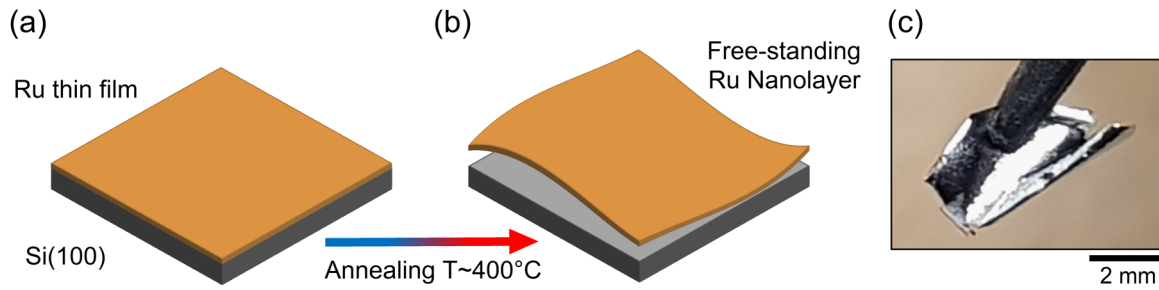


FIG. 1. Sketch of the delamination process. (a) Ru-based thin films (thickness ranging from approximately 20 up to 200 nm) are sputter deposited onto clean Si(100) substrates with native oxide. (b) Annealing at  $T \approx 400$  °C causes the delamination of the film from the substrate. (c) Centimeter-sized free-standing layer (200 nm Ru<sub>77</sub>Mo<sub>23</sub>) exfoliated from the substrate with tweezers.

splitting of 4.1 eV, and an asymmetric peak shape, in good agreement with reports for metallic Ru in the literature [28]. Moreover, the extended Ru 3d region in Fig. 2(a) shows the presence of a broad plasmon loss feature at a binding energy value of approximately 312 eV, corresponding to an electron energy difference of  $\Delta E \approx 32$  eV with respect to the main Ru 3d<sub>5/2</sub> peak.

In the XPS spectra of the thin-film side of the exfoliated Ru/Si(100) interface (red), the main Ru 3d<sub>5/2</sub> peak of the spectrum is shifted by 0.45 eV towards lower binding energy with respect to metallic Ru, comparable to the binding energy shift attributed to the formation of a metal-rich Ru silicide in the literature [29]. The extended Ru 3d region in Fig. 2(a) shows a plasmon loss peak at approximately 305 eV ( $\Delta E \approx 25.5$  eV), which is close to its position in the Ru silicide reference sample at 303 eV (blue). Moreover, the peak shape of the Ru 3d doublet of the thin-film side of the Ru/Si(100) interface spectrum in Fig. 2(b) shows a sharp contrast to the asymmetric shape that is characteristic of metallic Ru (black)

[28], and resembles the symmetric peak shapes of the Ru silicide Ru 3d doublet (blue). The increased width and shifted binding energy of the plasmon loss peak at the thin-film side of the Ru/Si(100) interface compared to the silicide reference as well as the small residual asymmetry of the Ru 3d peaks indicate the presence of a small amount of metallic Ru close to the interface. This comparison indicates a change in electronic structure with the annealing treatment and suggests the formation of a nonmetallic Ru silicide at the interface between the Ru thin film and the substrate. A detailed XPS investigation to discern the type of silicide that is formed is beyond the scope of this study.

A survey spectrum of the thin-film side of the Ru/Si(100) interface reveals the presence of silicon and oxygen (Supplemental Material Fig. S2(a) [27]). From the measured XPS peak area we estimated the relative composition of Ru, Si, and O in the surface region to be 39.5%, 39.1%, and 21.4%, respectively, as reported in Fig. 2(c). Variations in probing depth with different electron kinetic energies were not taken

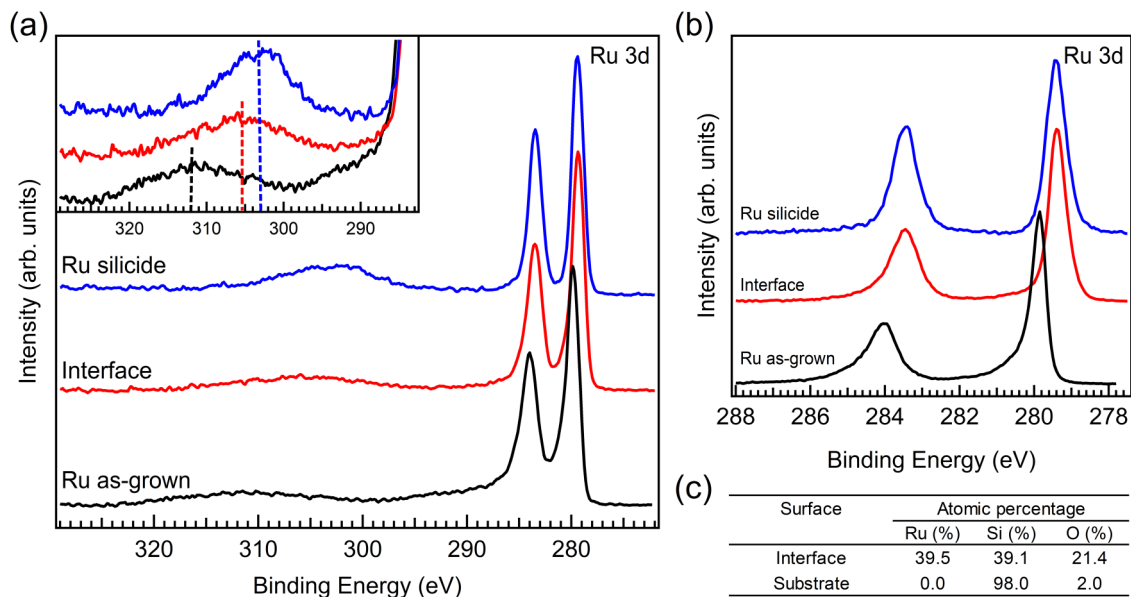


FIG. 2. XPS results of the Ru layer before and after delamination. (a) Extended Ru 3d region of the as-grown Ru thin film (black), the thin-film side of the Ru/Si(100) interface after annealing and tape delamination in UHV (red), and a Ru silicide thin-film reference (blue). The shift of the plasmon loss peak maximum is highlighted in the inset with dashed lines. (b) Ru 3d detailed spectra of the as-grown Ru thin film (black), thin-film side of the Ru/Si(100) interface (red), and Ru silicide reference (blue). (c) Surface compositions of the thin-film side of the Ru/Si(100) interface and the Si(100) substrate after annealing and exfoliation in UHV.

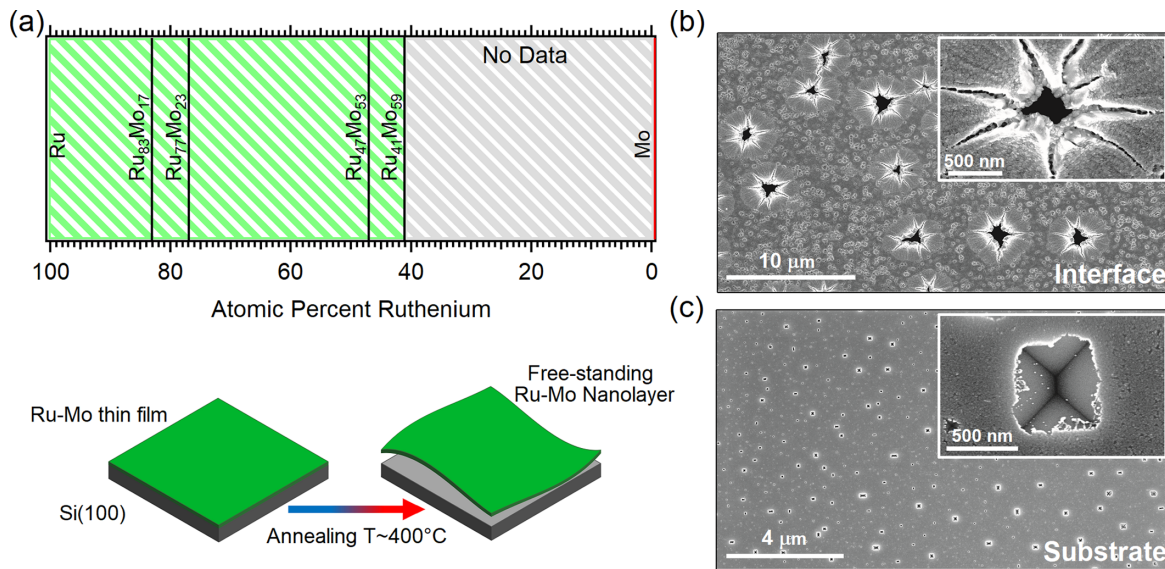


FIG. 3. (a) Schematic summary of the different Ru-Mo thin films investigated. The production of free-standing Ru-Mo nanolayers (sketch at the bottom) was successful for pure Ru and all alloy compositions in this study (green area). For pure Mo (red line) no delamination was observed. (b) SEM micrograph of a 200 nm thick Ru<sub>77</sub>Mo<sub>23</sub> film, delaminated upon annealing at 700 °C and viewed from the side that had been in contact with the Si(100) substrate. (c) SEM micrograph of the Si(100) substrate after annealing and exfoliation of the same Ru<sub>77</sub>Mo<sub>23</sub> film.

into account. The detailed spectrum of the Si  $2p$  region [Fig. S2(b)] shows a small shift of the main Si  $2p_{3/2}$  peak of 0.3 eV towards a higher binding energy value compared to elemental Si, which is in agreement with literature on Ru silicide [29]. The presence of SiO<sub>2</sub> was only observed on the thin-film side of the delaminated Ru/Si(100) interface, whereas on the substrate the signal from SiO<sub>x</sub> species was below the detection limit in the Si  $2p$  region [Figs. S2(c) and S2(d)] and the O  $1s$  signal was very low [ $\leq 2\%$ , see Fig. 2(c)]. In the region probed by XPS, the thin-film side of the Ru/Si(100) interface exhibited a ratio of oxidized silicon to the sum of Ru and total Si of SiO<sub>x</sub>/(Ru + Si<sub>tot</sub>)  $\approx 20\%$ , a value that is higher than the SiO<sub>2</sub>/Si<sub>tot</sub> ratio measured for a Si(100) substrate with native oxide (approximately 11%). No traces of ruthenium were detected on the substrate after the delamination. We conclude that the native oxide delaminated from the substrate together with the Ru thin film in its entirety and remained at least partly intact. The higher SiO<sub>2</sub> signal on Ru silicide is attributed to a shorter inelastic mean-free path of photoelectrons in the Ru silicide layer, which led to a lower measured intensity of Ru and Si. These observations indicate a sharp separation at the Si-SiO<sub>2</sub> interface with negligible intermixing after Si diffusion.

We tested whether or not the observed delamination behavior is specific for Ru layers on Si(100) by repeating the same procedure for Mo and for Ru-Mo alloys of four different compositions (Ru<sub>100-x</sub>Mo<sub>x</sub>). In addition to the effect of composition, the study of Ru-Mo alloys allowed us to assess the effect of structural disorder, since a high Ru content was reported to favor the growth of polycrystalline films, while approximately equiatomic compositions were found to assume an amorphous structure for deposition at room temperature [30]. Figure 3(a) summarizes the observed effect of composition and structure on the delamination of Ru-Mo films. Reproducible delamination was achieved for all five

investigated Ru-containing compositions (pure Ru to Ru<sub>41</sub>Mo<sub>59</sub>), proving that the effect is not limited to a narrow compositional range or a certain crystallographic structure. For pure Mo, we did not succeed in producing free-standing nanolayers by delamination from the substrate up to annealing temperatures of 700 °C [red line in Fig. 3(a)]. No other indications of reduced adhesion were observed for the annealed Mo films. We therefore conclude that for the binary Ru-Mo system the presence of Ru is essential for the reported delamination mechanism.

The necessary ingredients for delamination were further explored by varying the substrate properties and deposition technique. No delamination was observed for Ru films on Si(100) without its native SiO<sub>2</sub> layer, which had been removed via etching with hydrofluoric acid. Thicker interlayers of SiO<sub>2</sub> (approximately 20 nm), achieved by annealing the substrates in air, also prevented delamination, most likely by inhibiting Si diffusion. The orientation of the substrate plays a decisive role as well, demonstrated by annealing Ru layers on native-oxide terminated Si(111), for which no tendency towards lower adhesion was observed. Also a change in deposition method to pulsed laser deposition (PLD) in UHV modified the Ru/SiO<sub>2</sub>/Si(100) sufficiently to avoid delamination, whereas silicide formation was still observed upon annealing. The highly reproducible effect observed on sputter-deposited Ru/SiO<sub>2</sub>/Si(100) was thus found to be strongly affected by small variations in interface properties, such as surface energy, defect density, and diffusivity in the oxide layer.

Figures 3(b) and 3(c) show scanning electron microscopy (SEM) images of the free-standing film at the thin-film side of the Ru/Si(100) interface [Fig. 3(b)] and of the substrate [Fig. 3(c)] after delaminating a 200 nm thick Ru<sub>77</sub>Mo<sub>23</sub> film. The thin-film side of the Ru/Si(100) interface is imaged as a smooth surface with nanoscale speckles that we attribute to small crystallites in the annealed silicide layer. The most

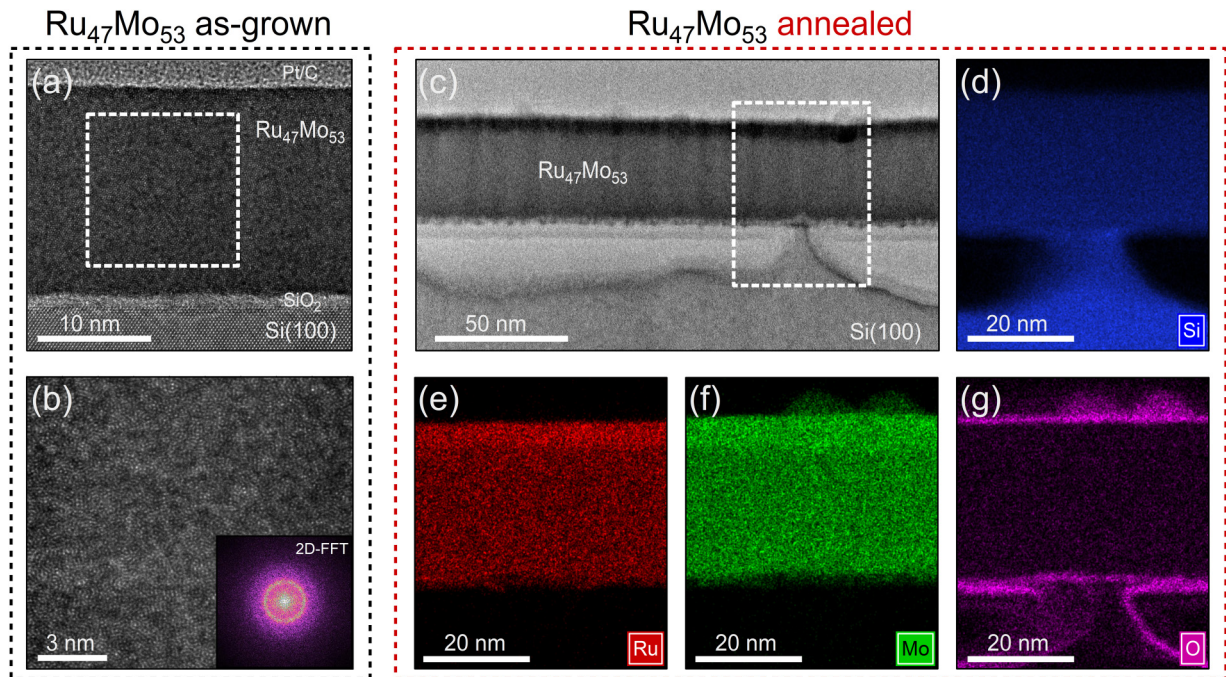


FIG. 4. HR-TEM measurements of a 20 nm thick  $\text{Ru}_{47}\text{Mo}_{53}$  thin film. (a) TEM image of the as-grown sample showing the crystalline Si(100) substrate, the disordered native  $\text{SiO}_2$ , and the amorphous metallic thin film. (b) Zoomed-in region of the  $\text{Ru}_{47}\text{Mo}_{53}$  thin film [white square in (a)], and corresponding 2D-FFT filtered using a Hann function (inset), both adapted from Yetik *et al.* [30]. (c) TEM image of the  $\text{Ru}_{47}\text{Mo}_{53}$  thin film after annealing at 400 °C. (d)–(g) EDX maps of the white dashed rectangular area in (c) for Si, Ru, Mo and O.

prominent features in the images are micrometer-sized protrusions with a volcanolike shape, characterized by a thin cracked layer lifted off the film and a dark “crater.” A large fraction of the electrons from this central region is prevented from reaching the detector, which is positioned at an angle of approximately 30° with respect to the sample surface, resulting in a lack of signal. The volcanolike appearance indicates a violent process of formation, breaking up a thin overlayer of the Ru-based film by pulling (or pushing) it upwards. We propose that these structures form during the exfoliation step at locations where the film is still connected to the substrate after annealing. The strong adhesion at these “defects” leads to a local breakup of an overlayer upon mechanical exfoliation. In Fig. 3(c) a SEM micrograph of the substrate after exfoliation shows the presence of a high number of rectangular cavities. The zoomed-in image in the inset reveals that these cavities have the shape of inverse pyramids of missing silicon in the single-crystalline Si(100) substrate. In the context of the silicide formation reported above, it is likely that these inverse pyramids are etch pits, which have been observed as a result of silicide formation on Si(100) for several metals [31,32]. Typically the faces of the pyramids follow the crystal plane with the lowest surface energy. For Si, these are the {111} planes [33], which form facets at an angle of 54.7° with respect to the (100) plane [34].

The high-resolution transmission electron microscopy (HR-TEM) measurements of a 20 nm thick  $\text{Ru}_{47}\text{Mo}_{53}$  thin film in Fig. 4 provide mechanistic insights into the delamination process. Figure 4(a) shows a cross-sectional high-resolution TEM image of the as-grown amorphous  $\text{Ru}_{47}\text{Mo}_{53}$  thin film on a Si(100) substrate with native  $\text{SiO}_2$  layer. The topmost layer labeled Pt/C is required for TEM sample

preparation using focused-ion-beam cutting. In Fig. 4(b) a zoomed-in section of the  $\text{Ru}_{47}\text{Mo}_{53}$  thin film is reported, highlighted with a dashed square in Fig. 4(a). The complete lack of long-range order is evident in the image and can also be inferred from the two-dimensional fast Fourier transform (2D-FFT) pattern in the inset. The absence of preferred orientations and of long-range order results in a broad ring without sharp features in reciprocal space [30]. The right-hand side of Fig. 4 shows HR-TEM images of the  $\text{Ru}_{47}\text{Mo}_{53}$  thin film after annealing. The image in Fig. 4(c) shows that the amorphous Ru-Mo film has detached from the Si(100) surface with annealing at 400 °C. The light gray region between the Ru-Mo layer and the Si substrate corresponds to empty space created by the detachment of the alloy layer. The darker shaded regions close to the substrate and the metal film are a result of oxidation and carbon accumulation during focused-ion-beam cutting (see also Fig. S6 [27]). A detailed image of the amorphous Ru-Mo layer after annealing is available in Fig. S3 [27]. The dashed white box in Fig. 4(c) highlights one of the few locations where the nanolayer remained locally attached to the substrate since no mechanical force was applied to complete the exfoliation. The composition of the highlighted region was investigated using energy-dispersive x-ray spectroscopy (EDX) maps of Ru, Mo, Si, and O in Figs. 4(d)–4(g). These measurements reveal the diffusion of silicon from the substrate into the alloy thin film with annealing. The delaminated Ru-Mo layer contains a substantial fraction of Si, whereas the as-deposited Ru-Mo film contains no Si (Fig. S4 [27]). On the other hand, no diffusion of Ru and Mo to the Si substrate was observed, as shown in Figs. 4(e) and 4(f), respectively. In addition to the change in composition, the TEM measurements show that the thickness of the metallic thin film has increased

from 20 nm before annealing [Fig. 4(a)] to approximately 32–33 nm afterwards [Fig. 4(c)], corresponding to a swelling by more than 60% with respect to the as-grown film.

In addition to the production of Ru-based membranes, we demonstrate that Ru delamination can serve as a pathway to achieve free-standing layers of custom composition. Very thin Ru buffer layers were found sufficient to enable the exfoliation of free-standing metal nanolayers. For sputter-deposited, 200 nm thick Mo films, a Ru buffer layer of only 5 nm thickness was enough to enable exfoliation after annealing at 600 °C. The characteristic change in reflectivity that indicates the detachment from the substrate was observed already at around 400 °C. For a 45 nm thick film of the high-entropy alloy HfMoNbTiZr (20:20:20:20:20 at.%) deposited using PLD, no delamination occurred for 5 nm Ru, but successful exfoliation of an intact stack of HfMoNbTiZr/Ru/SiO<sub>2</sub> [Fig. S5(a)] was achieved for a 20 nm thick Ru buffer layer. We attribute the higher required thickness to intermixing of the deposited HfMoNbTiZr with the thin Ru layer upon deposition, caused by the high kinetic energy of the material arriving at the surface during the PLD process. XPS spectra of successfully delaminated films showed only Ru and Si close to the interface with the Si substrate [Fig. S5(b)], indicating that no significant alloying between Ru and other metals in the stack occurred at the temperature required for delamination.

The combined evidence from *in situ* XPS, visual observation during annealing, HR-TEM, EDX, and SEM enables us to propose a qualitative delamination mechanism. Already at 400 °C, Si atoms diffuse through the native SiO<sub>2</sub> layer on Si(100) into the Ru film. The formation of Ru silicide is thermodynamically favorable and readily proceeds at 400 °C, leading to the incorporation of substantial amounts of Si. The incorporated Si results in swelling of the film and the buildup of in-plane compressive stress. However, with all bonds at the interface intact, the barrier for cleaving is high and the Ru/SiO<sub>2</sub>/Si structure remains intact. However, if the layer detaches in one location, for example at one of the pyramidal cavities in the Si substrate, the layer can buckle to locally release the compressive stress caused by Si incorporation. The atoms directly adjacent to this detached region experience a strong localized force pulling them off the substrate in addition to the high compressive stress in the layer. This combination results in the breaking of bonds and the growth of the delaminated region, which propagates across the sample in an avalanchelike manner. The *in situ* XPS results confirm that the breaking point is the interface between Si(100) and SiO<sub>2</sub>. This interface is expected to be the energetically most favorable one to cleave, based on reports of the surface energies of low-index Si surfaces [35], their native SiO<sub>2</sub> layers [36], and on a higher surface energy of Ru silicide compared to Si(111) [37]. The delaminated layer remains attached to the substrate at a small number of locations, for example at defects leading to crystallization of particles at the interface, and is removed upon mechanical exfoliation.

The HR-TEM images support the proposed mechanism in several respects. In combination with EDX, they provide information on the diffusing species, the presence of the native oxide, and the total layer thickness. The EDX results demonstrate that annealing treatment results in the diffusion of silicon into the film, whereas no indications for metal

diffusion are observed, which is the dominant mechanism of silicide formation for several transition metals such as Ni [38]. The images further indicate that the native oxide layer remains largely intact, which is also confirmed using *in situ* XPS. In Fig. 4(g) the oxide layer appears to be thinner and shows spatial variations in density at the connecting point between film and substrate: this observation indicates that defects in the silicon native oxide may facilitate the diffusion of Si. This is particularly relevant since no Si diffusion in amorphous silica is expected at 400 °C [39], in agreement with the absence of the delamination effect for Ru on thicker SiO<sub>2</sub> layers at otherwise comparable conditions. The formation of silicide thus indicates that the native oxide is either sufficiently thin to allow for Si diffusion or locally damaged, for example during sputter deposition, where energetic ions can create defects that act as diffusion channels and define the starting points of silicide formation. According to the TEM results, however, the Si is not localized to a small number of channels but homogeneously distributed in the metal film converted to silicide. This conversion leads to a considerable increase in equilibrium volume (from about 0.014 to 0.034 nm<sup>3</sup>/Ru for the example of Ru<sub>2</sub>Si<sub>3</sub>) [40], which exceeds the thermal expansion of all materials in this study over the relevant temperature range by several orders of magnitude. This increase in volume is borne out by a substantially larger film thickness (by ≈60%) observed in TEM images. In-plane expansion, however, is blocked by bonds at the interface, preventing full equilibration of the volume and creating extrinsic compressive stress in the layer [25]. This is in agreement with the observed buckling upon delamination.

The proposed mechanism further highlights that all three components of the Ru/SiO<sub>2</sub>/Si(100) stack are imperative for the delamination to occur. The interface between Si(100) and its thin native SiO<sub>2</sub> layer is crucial as the location of separation, indicated by the unsuccessful attempts to generalize the effect to modified interfaces, for example without SiO<sub>2</sub>, with a thicker SiO<sub>2</sub> layer, or with different surface orientation of Si. An oxide layer of finite thickness is essential for the detachment, since it ensures a favorable cleavage point with low-energy surfaces for both the substrate and the free-standing film. The absence of oxygen from the Si(100) substrate indicates the preference to cleave at a well-defined plane, minimizing the roughness and number of broken Si-O bonds. The importance of an intact SiO<sub>2</sub>-Si interface and oxide layer is highlighted by the absence of delamination for pulsed laser deposited films, which most likely grow on an oxide that is damaged by high-energy atoms and ions during the deposition process. The relevance of the surface orientation is most likely related to the removal of Si from the surface layer. In the case of Si(100), this removal leads to the formation of cavities with {111}-oriented faces, which are not expected to occur in the same way on Si(111) but could have an essential role, for example as starting points for the detachment and buckling of the film. The importance of the element Ru is clear from the reported observations, but the reasons for this selectivity remain unclear. The preference for Si as a diffusing species in the formation of Ru silicide establishes a clear difference to other transition metals such as Ni [38]. The tendency of Ru to form silicides with significantly larger volume at low temperature is not sufficiently different from

Mo [41] to explain the observed selectivity. The preference of Ru for hexagonal structures is not expected to play a decisive role based on the observed delamination of amorphous Ru-Mo layers. We speculate that a strong interfacial adhesion at the Ru-SiO<sub>2</sub> interface mediates the transfer of strain to the SiO<sub>2</sub>-Si(100) interface, potentially related to the coexistence of Ru silicide and small metallic contributions observed in XPS of the thin-film side of the delaminated Ru/Si(100) interface.

Finally, the templating experiments with thin Ru buffer layers can also be explained with the same mechanism. The results indicate that Ru is essential at the interface, but already 5 nm of Ru buffer layer is sufficient to allow for major modifications of the metal film without interfering with the delamination. The increase in required thickness for the high-entropy alloy deposited using PLD, a deposition technique with high-energy particles impinging at the surface, indicates that an intact interface with SiO<sub>2</sub> and a minimum thickness of continuous Ru in the first nanometers of the film is essential. For Ru thicknesses surpassing a critical value, the process is expected to be independent of the deposition technique and should even allow for growth in reactive atmosphere and at elevated temperature, provided the Ru layer remains intact and silicide formation does not occur before inducing delamination. Moreover, this approach could also be applicable to other functional materials, such as oxides, other ceramics, and high-temperature polymers.

#### IV. CONCLUSIONS

Our results demonstrate that annealing thin Ru-based films on Si(100) with native oxide leads to the delamination of

centimeter-sized free-standing nanolayers, which detach from the substrate at the sharp interface between Si and its native oxide. We propose an explanation of the effect based on stress caused by the conversion of the Ru layer to Ru silicide, concomitant with a strong increase in the equilibrium volume of the film and the buildup of compressive stress. The layer responds by buckling, starting locally at pyramidal cavities in the Si substrate. Once the layer can detach locally, which is easiest at the pyramidal cavities in the Si substrate, it starts buckling. The detached region grows in an avalanchelike manner, creating an ultrathin free-standing membrane and leaving behind a clean Si substrate. We demonstrate that the delamination effect can be generalized to the pure metal Mo and the PLD-grown complex alloy HfMoNbTiZr by making use of thin Ru buffer layers. The delamination of Ru-supported layers thus shows potential to enable the chemical-free fabrication of metal nanolayers of custom composition. This approach is compatible with a variety of deposition techniques and growth conditions as well as fully vacuum-based processing, while remaining simple and environmentally friendly.

#### ACKNOWLEDGMENTS

This work has been carried out at the Advanced Research Center for Nanolithography, a public-private partnership of the University of Amsterdam, the Vrije Universiteit Amsterdam, the Dutch Research Council (NWO), and the semiconductor equipment manufacturer ASML.

- 
- [1] Y. Liang, S. Zhang, X. Cao, Y. Lu, and T. Xu, *Sci. Rep.* **7**, 4357 (2017).
- [2] F. R. Powell, P. W. Vedder, J. F. Lindblom, and S. F. Powell, *Opt. Eng.* **29**, 614 (1990).
- [3] K. Jimenez, P. Nicolosi, L. Juschkina, N. Ahmed, A. E. Gaballah, E. Cattaruzza, M. G. Sertso, A. Gerardino, A. Giglia, G. Mussler, and P. Zuppella, *Thin Solid Films* **695**, 137739 (2020).
- [4] K. Han, L. Wu, Y. Cao, H. Wang, C. Ye, K. Huang, M. Motapothula, H. Xing, X. Li, D. C. Qi, X. Li, and X. Renshaw Wang, *ACS Appl. Mater. Interfaces* **13**, 16688 (2021).
- [5] B. S. Yin, Z. B. Wang, S. W. Zhang, C. Liu, Q. Q. Ren, and K. Ke, *ACS Appl. Mater. Interfaces* **8**, 26019 (2016).
- [6] R. Govind and D. Atnoor, *Ind. Eng. Chem. Res.* **30**, 591 (1991).
- [7] S. Adhikari and S. Fernando, *Ind. Eng. Chem. Res.* **45**, 875 (2006).
- [8] C. Zoldesi, K. Bal, B. Blum, G. Bock, D. Brouns, F. Dhalluin, N. Dziomkina, J. D. A. Espinoza, J. de Hoogh, S. Houweling, M. Jansen, M. Kamali, A. Kempa, R. Kox, R. de Kruif, J. Lima, Y. Liu, H. Meijer, H. Meiling, I. van Mil *et al.*, *Extreme Ultraviolet (EUV) Lithography V* **9048**, 90481N (2014).
- [9] E. E. Gallagher, J. Vanpaemel, I. Pollentier, H. Zahedmanesh, C. Adelman, C. Huyghebaert, R. Jonckheere, and J. U. Lee, *Photomask Technol.* **2015** **9635**, 96350X (2015).
- [10] D. L. Goldfarb, *Photomask Technol.* **2015** **9635**, 96350A (2015).
- [11] H. J. Shin, I. S. Park, Y. J. Jang, S. J. Wi, G. S. Lee, and J. Ahn, *Sens. Actuators, A* **297**, 111538 (2019).
- [12] X. Kong, K. Xu, C. Zhang, J. Dai, S. Norooz Oliaee, L. Li, X. Zeng, C. Wu, and Z. Peng, *ACS Catal.* **6**, 1487 (2016).
- [13] H. Liu, C. Xi, J. Xin, G. Zhang, S. Zhang, Z. Zhang, Q. Huang, J. Li, H. Liu, and J. Kang, *Chem. Eng. J.* **404**, 126530 (2021).
- [14] K. H. Seng, J. Liu, Z. P. Guo, Z. X. Chen, D. Jia, and H. K. Liu, *Electrochem. Commun.* **13**, 383 (2011).
- [15] N. Luo, G. J. Ji, H. F. Wang, F. Li, Q. C. Liu, and J. J. Xu, *ACS Nano* **14**, 3281 (2020).
- [16] Y. L. Ding, Y. Wen, P. A. Van Aken, J. Maier, and Y. Yu, *Small* **11**, 2011 (2015).
- [17] N. Setter, *Electroceramic-Based MEMS*, edited by N. Setter (Springer US, New York, 2005), pp. 348
- [18] J. A. Thornton, *Thin Solid Films* **171**, 5 (1989).
- [19] M. F. Doerner and W. D. Nix, *Crit. Rev. Solid State Mater. Sci.* **14**, 225 (1988).
- [20] K. Kinoshita, *Thin Solid Films* **12**, 17 (1972).
- [21] B. Lu, Y. Song, Z. Guo, and J. Zhang, *Int. J. Solids Struct.* **50**, 2495 (2013).
- [22] R. Mainz, H. Rodriguez-Alvarez, M. Klaus, D. Thomas, J. Lauche, A. Weber, M. D. Heinemann, S. Brunken, D. Greiner, C. A. Kaufmann, T. Unold, H. W. Schock, and C. Genzel, *Phys. Rev. B* **92**, 155310 (2015).



- [23] Y. Kuru, M. Wohlschlägel, U. Welzel, and E. J. Mittemeijer, *Thin Solid Films* **516**, 7615 (2008).
- [24] P. Gas and F. M. D'Heurle, *Appl. Surf. Sci.* **73**, 153 (1993).
- [25] O. Thomas, P. Gergaud, C. Rivero, and F. D'Heurle, *Defect Diffusion Forum* **237-240**, 801 (2005).
- [26] V. E. Borisenko, *Semiconducting Silicides*, 1st ed. (Springer, Berlin, 2000), p. 50
- [27] See Supplemental Material at <http://link.aps.org/supplemental/10.1103/PhysRevMaterials.6.043402> for a movie of the change in appearance of a Ru thin film during annealing, XPS survey and Si 2p spectra of the delaminated interface, and TEM images as well as TEM-EDX results of an annealed Ru-Mo alloy layer.
- [28] D. J. Morgan, *Surf. Interface Anal.* **47**, 1072 (2015).
- [29] L. Pasquali, N. Mahne, M. Montecchi, V. Mattarello, and S. Nannarone, *J. Appl. Phys.* **105**, 044304(2009).
- [30] G. Yetik, A. Troglia, S. Farokhipoor, S. Van Vliet, J. Momand, B. J. Kooi, R. Bliem, and J. M. W. Frenken, *arXiv:2204.04126* (2022).
- [31] K. Park and K. Kim, *J. Electrochem. Soc.* **142**, 3109 (1995).
- [32] G. H. Shen, J. C. Chen, C. H. Lou, S. L. Cheng, and L. J. Chen, *J. Appl. Phys.* **84**, 3630 (1998).
- [33] R. J. Jaccodine, *J. Electrochem. Soc.* **110**, 524 (1963).
- [34] A. A. Baski, S. C. Erwin, and L. J. Whitman, *Surf. Sci.* **392**, 69 (1997).
- [35] A. A. Stekolnikov, J. Furthmüller, and F. Bechstedt, *Phys. Rev. B* **65**, 115318 (2002).
- [36] S. R. Narayan, J. M. Day, H. L. Thinakaran, N. Herbots, M. E. Bertram, C. E. Cornejo, T. C. Diaz, K. L. Kavanagh, R. J. Culbertson, F. J. Ark, S. Ram, M. W. Mangus, and R. Islam, *MRS Adv.* **3**, 3379 (2018).
- [37] M. Toramaru, N. Kobayashi, N. Kawamura, S. Ohno, Y. Miyamoto, and K. Shudo, *Surf. Interface Anal.* **45**, 1109 (2013).
- [38] M. Liehr, H. Dallaporta, and J. E. Lewis, *Appl. Phys. Lett.* **53**, 589 (1988).
- [39] M. L. F. Nascimento and E. D. Zanotto, *Phys. Chem. Glasses: Eur. J. Glass Sci. Technol., Part B* **48**, 201 (2007).
- [40] D. Poutcharovsky and E. Parthé, *Acta Crystallogr., Sect. B* **30**, 2692 (1974).
- [41] I. Nedelcu, R. W. van de Kruijs, A. E. Yakshin, and F. Bijkerk, *J. Appl. Phys.* **103**, 083549 (2008).